Chisté *et al. Chem. Biol. Technol. Agric.* (2024) 11:154
https://doi.org/10.1186/s40538-024-00645-2

Chemical and Biological Technologies in Agriculture

RESEARCH

Open Access

Biochar-boron composites: synthesis, properties and agronomic effectiveness for eucalyptus seedlings

Loren Chisté[1], Leônidas Carrijo Azevedo Melo[1*], Keiji Jindo[2*] and Carlos Alberto Silva[1*]

Abstract

Introduction Boron (B) is critical for plant growth, yet its movement in soil is often hindered by leaching and adsorption, leading to deficiencies. Tackling these issues is essential for boosting agricultural productivity, especially in plants like Eucalyptus with high B needs. This paper aims to address these challenges by evaluating B-doped biochar composites (biochar-B) that enhance B distribution and stability in the soil, focusing on *Eucalyptus grandis* cultivation in two distinct oxisol types.

Materials and methods Biochar-B composites were created using shrimp carcass (FSC), chicken manure (FCM) and sewage sludge (FSS), combined with boric acid (BA) and borax (BX), and pyrolyzed at 300 °C and 550 °C. The experimental design was a completely randomized design (CRD) with three replicates.

Results Fourier transform infrared spectroscopy (FTIR) analysis confirmed successful B integration and interaction with organic matrices, highlighting functional groups responsible for composite properties. This facilitated the development of highly predictive partial least squares (PLS) regression models (R^2pred ~ 0.8). The FSC-BA composite at 300 °C showed notable thermal stability, B retention and availability, enhancing B release kinetics.

Discussion These findings emphasize the importance of considering the soluble B rate in composite applications for Eucalyptus cultivation. The use of these composites provides a sustainable method for gradual B release, potentially outperforming conventional fertilization techniques. This approach may lead to improved plant growth and productivity. Further field investigations are recommended in order to validate these findings and refine sustainable fertilization strategies; thus, benefiting a range of crops.

Keywords B-carbon complexes, Pyrolysis conditions, Kinetics of B release, FTIR, B availability in soil

*Correspondence:
Leônidas Carrijo Azevedo Melo
leonidas.melo@ufla.br
Keiji Jindo
keiji.jindo@wur.nl
Carlos Alberto Silva
csilva@ufla.br
Full list of author information is available at the end of the article

Graphical abstract

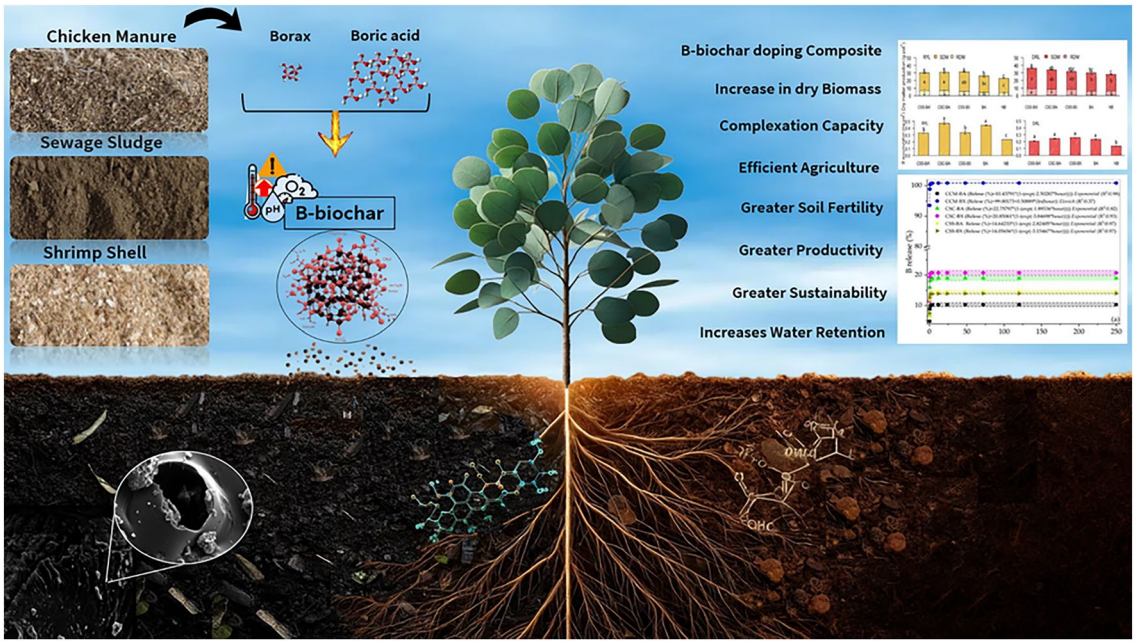

Introduction

Boron (B) is a vital trace element for numerous biochemical and physiological processes in plants. It plays a pivotal role in functions such as nucleic acid synthesis, chlorophyll formation, protein synthesis, carbohydrate transport, pollen tube growth and root development [1]. Its deficiency in soil can hinder water uptake, resulting in the desiccation of growth tissues. This scenario is especially evident in eucalyptus species during drought periods [2]. Such deficiency not only obstructs reforestation efforts but also diminishes the commercial value of eucalyptus timber, which requires a substantial amount of B to thrive [3]. However, ensuring adequate B levels in soil presents a significant challenge due to the swift depletion of traditional B supplements, highlighting the urgent need for more reliable and effective B supplementation methods.

Boron availability in soil is influenced by factors like pH, B source solubility, adsorption, complexation and transportation involving organic matter, metal hydroxides, and clay minerals [4]. The precise evaluation of B fractions faces challenges due to the intricate characteristics of soils and constraints in extraction techniques. These challenges often result in inconsistent B release kinetics, having an impact on the nutritional management of eucalyptus plantations [5]. B-doped biochar has shown promise in enhancing electron transfer rates, acting as an efficient carbon (C) catalyst without metal components [6]. However, research on the influence of composites on the solubility and stability of B–C complexes within carbonized matrices, as well as the dynamics of B release from these materials for fertilization purposes in different soil types, remains limited. The production of B-doped biochar focuses on stable B–C interactions through complexation [7] and chelation [8], affecting structural properties and functional group density [9], offering a novel approach to B fertilization efficiency via the B adsorption mechanism when associated with biochar [10].

The selection of feedstocks and pyrolysis temperatures is crucial, influencing B and C interactions and, thus, nutrient bioavailability in soil and plants [9]. Selecting ash-rich sources such as shrimp shells, chicken manure and sewage sludge is strategic, leveraging their capacity to produce biochars with fertilizing benefits [11–13], which is key to advancing sustainable agricultural methods. Generally, these wastes are discarded in landfills or used for composting, animal feed and soil amendments. Nevertheless, converting them into biochar not only mitigates waste disposal issues but also fully harnesses their high-value properties. This process enhances nutrient cycling efficiency, improves soil health and reduces potential environmental impacts. High-temperature processes enable B

to form stable covalent bonds with C, enhancing biochar structural and functional qualities [14]. The incorporation of boric acid (BA) and sodium borate (borax) (BX) not only bolsters biochar's thermal and physicochemical properties [15] but also holds an agricultural purpose as a nutrient. This research explores the B–C interaction within biochar, which is essential for controlled releases and the improvement of soil fertility. Through the investigation of composites, we aim to redefine sustainable agriculture by fine-tuning biochar properties, showcasing innovation within agricultural functionalities and opening pathways for more sustainable farming practices. Oxisol was selected for this study because it is the most common soil order in tropical regions and is widely affected by B deficiency, posing significant challenges for B management in plant nutrition. This study examines the production of composites from FCM, FSC and FSS doped with BA and BX, pyrolyzed at temperatures from 300 °C to 550 °C. The main intent is to assess the kinetics of B release to optimize its utilization by eucalyptus seedlings while minimizing leaching, thereby enhancing the efficiency of B fertilizers. Additionally, FTIR-based prediction models are utilized to understand chemical interactions between B and C atoms during pyrolysis, with focus on elucidating environmental processes, remediation strategies, organic waste utilization and nutrient cycling management in Oxisols.

Table 1 Identification of feedstocks, B sources and abbreviated temperatures of synthesized biochar composites

Acronym	Feedstock	B source
Temperature 60 °C		
FCM	Chicken manure	No
FSC	Shrimp carcass	
FSS	Sewage sludge	
Pyrolysis temperature—300 °C		
BCM	Chicken manure	No
BSC	Shrimp carcass	
BSS	Sewage sludge	
CCM-BA	Chicken manure	Boric acid
CCM-BX		Borax
CSC-BA	Shrimp carcass	Boric acid
CSC-BX		Borax
CSS-BA	Sewage sludge	Boric acid
CSS-BX		Borax
Pyrolysis temperature—550 °C		
BCM′	Chicken manure	No
BSC′	Shrimp carcass	
BSS′	Sewage sludge	
CCM-BA′	Chicken manure	Boric acid
CCM-BX′		Borax
CSC-BA′	Shrimp carcass	Boric acid
CSC-BX′		Borax
CSS-BA′	Sewage sludge	Boric acid
CSS-BX′		Borax

Material and methods

Preparation and characterization of the feedstocks

We selected three feedstocks for the synthesis of biochars and their composites: chicken manure (FCM), shrimp shell (FSC) and municipal sewage sludge (FSS). The FCM was sourced from an agricultural facility in Nepomuceno, Minas Gerais, Brazil, (Latitude: − 21.236110° S; Longitude: − 45.234970° W). The FSS was obtained from a treatment facility at the Universidade Federal de Lavras, located in Lavras, Minas Gerais, Brazil (Latitude: − 21.23008° S; Longitude: − 44.98981° W). The FSC were procured from a marine processing enterprise in Linhares, Espírito Santo, Brazil (Latitude: − 19.373030° S; Longitude: − 40.054680° W). Comprehensive specifications for each material are delineated in Table 1.

Initially, the feedstocks were subjected to air drying at room temperature in order to eliminate surface moisture. This was followed by subsequent dehydration in a forced air oven at 65 °C until a constant mass was reached. After drying, the samples were ground and passed through a sieve to obtain a uniform particle diameter of less than 0.25 mm. To inhibit rehumidification, the processed materials were subsequently stored in hermetically sealed plastic containers.

Preparation of biochar and B-doped biochar

Six distinct biochar specimens were produced utilizing the aforementioned feedstocks (FCM, FSC, and FSS) and two temperatures (300 °C and 550 °C). Additionally, twelve composites doped with B were created by incorporating boric acid (H_3BO_3) and borax ($Na_2B_4O_7$) obtained from ISOFAR and Exodus Scientific, aiming to reach a final B content of 7%. The pyrolysis process involved a controlled temperature increase at 10 °C/min up to the target temperatures (300 or 550 °C), using a muffle furnace equipped with an airtight chamber to block oxygen infiltration. This temperature was maintained for 60 min, then gradually cooled to room temperature before the furnace was opened. Subsequently, the biochar and composite samples were pulverized and sifted to obtain a particle size below 0.25 mm, which were then meticulously preserved for subsequent analysis.

Characterization of biochars and composites

Equations (1, 2 and 3) were employed to calculate volatile matter (VM), moisture (M) and ash content (As) of biochar using a modified ASTM D1762-84 method designed specifically for biochar analysis. This adaptation included pre-firing crucibles, heating them to 750 °C for six hours and cooling them to 105 °C to fully volatilize any remaining binders before the analysis took place [16]. The residue left after burning indicated the ash content (Ash) as described in Eq. (3). Fixed carbon (FC) was calculated based on Eq. (4) and the biochar yield (Y) was assessed using Eq. (5) [17].

$$\mathrm{VM}(\%) = \frac{\mathrm{DW\ at\ 105\,^{\circ}C} - \mathrm{DW\ at\ 950\,^{\circ}C}}{\mathrm{DW\ at\ 105\,^{\circ}C}} \times 100. \quad (1)$$

$$M(\%) = \frac{\mathrm{RW} - \mathrm{DW\ at\ 105\,^{\circ}C}}{\mathrm{RW}} \times 100. \quad (2)$$

$$\mathrm{Ash}(\%) = \frac{\mathrm{RW} - \mathrm{DW\ at\ 750\,^{\circ}C}}{\mathrm{DW\ at\ 105\,^{\circ}C}} \times 100. \quad (3)$$

$$\mathrm{FC}(\%) = \frac{\mathrm{DW\ at\ 105\,^{\circ}C} - \mathrm{DW\ at\ 950\,^{\circ}C} - \mathrm{DW\ at\ 750\,^{\circ}C}}{\mathrm{DW\ at\ 105\,^{\circ}C}} \times 100. \quad (4)$$

$$Y(\%) = 100 \times \frac{\mathrm{Biochar\ mass}}{\mathrm{105\ ^{\circ}C\ dried\ biomass}}. \quad (5)$$

The pH and electrical conductivity (EC) of the pyrolyzed matrices and feedstocks were measured using a digital pH meter (Toledo CE, Mettler-Toledo AG) precalibrated with pH 4 and 7 buffer solutions [18]. C content was determined using a Vario TOC cube analyzer via the dry combustion method. Total nitrogen (N) content was quantified by the Kjeldahl method following digestion with concentrated sulfuric acid [19]. Nutrient content was analyzed using inductively coupled plasma optical emission spectroscopy (ICP-OES) after digestion with a mixture containing sulfuric acid, potassium sulfate, copper sulfate and selenium (Table S1). Quality control was maintained using certified reference materials [19, 20] and blank samples in order to monitor for cross-contamination.

The levels of water-soluble B (W), 2% citric acid-soluble B (CA%) and neutral ammonium citrate (NAC) soluble B were determined via clear filtrate, following established protocols [21]. B concentration in the samples was obtained using ICP-OES analysis. To compare the B solubility of the samples, a B index was calculated, taking into account the ratio of the soluble fractions of B (B-W, B-NAC and B-CA%) and the total B content of each matrix, according to (Eq. 6).

$$\mathrm{B}(\%) = \frac{\mathrm{Soluble\ B\left(g.kg-1\right)}}{\mathrm{Total\ B\left(g.kg-1\right)}} \times 100. \quad (6)$$

Fourier transform infrared spectroscopy (FTIR)

Spectral signature characterization was performed in the mid-infrared region using an Agilent® Cary 630 FTIR spectrometer with a ZnSe-ATR crystal (Agilent Technologies, USA), with a scanning resolution of 4 cm^{-1}, in the wavelength range of 4000–650 cm^{-1}. Each FTIR spectrum was normalized [22]. The interpretation of the spectra and the identification of their respective spectral bands detected by the FTIR apparatus employed specific libraries and bands of biochars treated with B, described in [23].

Scanning electron microscope (SEM)

The scanning electron microscope (SEM) analysis was conducted using a JSM-7610F Schottky field emission scanning electron microscope (JEOL, Tokyo, Japan) at the Electron Microscopy and Ultrastructural Analysis Laboratory, within the Universidade Federal de Lavras Department of Phytopathology. Samples were prepared by oven drying 0.5 × 0.5 × 0.5 cm non-conductive pieces, mounting them on stubs with double-sided C tape and applying a C bath.

Boron release kinetics

A controlled incubation experiment was conducted to evaluate the kinetics of B release from pyrolyzed matrices. A composite sample weighing 1.0 g was transferred to a 50 mL container for incubation. Falcon tubes, combined with 20 mL of 0.1 mol L^{-1} citric acid (2% concentration) were horizontally stirred at 90 rpm and leachate was collected at predetermined intervals: 15 min, 30 min, 1 h, 2, 4, 12, 24, 48, 72, 120, and 250 h. After each extraction, the tubes were centrifuged for 5 min at 3500 rpm and the supernatant was collected for determination using ICP-OES.

Agronomic efficiency of the composites

The study was conducted at the Universidade Federal de Lavras, specifically in the Laboratory for the Study of Soil Organic Matter (LEMOS) at the Department of Soil Science, in Brazil. Eucalyptus seedlings were cultivated under greenhouse conditions using surface soil samples (0–20 cm) of representative Oxisols obtained within the university's campus and named dystrophic red-yellow

Table 2 The main chemical, physicochemical and texture characteristics of Oxisols used in eucalyptus cultivation

Oxisol	pH	C	Clay	Silt	Sand	N	P	K	Ca^{2+}	Mg^{2+}	B
		g kg^{-1}				mg dm^{-3}			Cmol dm^{-3}		mg dm^{-3}
RYL	4.7	4.5	460	85	455	329	6.1	218	0.8	0.4	0.1
DRL	4.5	19.8	770	100	130	2580	8.3	30.1	0.3	0.2	0.06

*RYL—red yellow latosol (medium texture); DRL—dystroferric red latosol; pH in a soil–water-Ratio of 1:2.5; C: C determined (dry combustion) in an automatic TOC analyzer; clay, silt and sand analyzed by the Bouyoucos method. All methods are described in detail [24]; N: total nitrogen—Kjeldahl; P: available phosphorus determined by the resin soil test; K, Fe^{2+}, Mn^{2+}, Cu^{2+} and Zn^{2+}: available determined by the $Mehlich^{-1}$ soil test; B: hot water extractor; exchangeable calcium (Ca^{2+}), exchangeable magnesium (Mg^{2+}) extracted by a 1 mol L^{-1} KCl solution soil test

latosol (RYL) and typical dystrophic red latosol (DRL). A detailed characterization is shown in Table 2.

The soil samples were air-dried, sieved (2 mm) and treated with calcium (Ca) and magnesium (Mg) carbonates ($CaCO_3$ and $MgCO_3$) in order to attain a pH of 5.5 ± 0.2 [24], so as to optimize conditions for eucalyptus growth and ensure Ca and Mg availability in the soils. The study employed a completely randomized design, with three feedstocks pyrolyzed at two temperatures and enriched with two B sources, totalling 12 B composites. Boron was applied to 1.8 mg kg^{-1} of soil using three replicates. Seedlings were planted in pots containing 3 kg of soil, which had additional fertilization with macro and micronutrients and irrigation was maintained at ~ 70% of the maximum water-holding capacity.

Soil solution samples from each pot were collected using Suolo Acqua® [25] at 1, 13, 28 and 70 days, filtered (< 0.45 µm) and measured for pH (Mettler Toledo benchtop pH meter) and B content via ICP-OES. Also, available B in soil (extracted in hot water) was determined using a spectrophotometer at the beginning (day 3) and at the end (day 100) of the experiment [24]. Subsequently, the plants were harvested, oven-dried at 65 °C for 72 h, their shoot dry matter (SDM) and root dry matter (RDM) were recorded, then they were ground in a mill (< 1 mm) and digested in a mixture of nitric and perchloric concentrated acids [26] whilst B was measured in ICP-OES. B uptake in the shoot dry matter of Eucalyptus (g) was calculated by multiplying the total nutrient content in the plant tissue (mg g^{-1}).

Statistical analysis

Data was submitted through a two-way ANOVA and when there was a significant difference ($p < 0.05$), the means of the treatments were compared with each other using Tukey's test ($p < 0.05$) (after meeting the ANOVA's analysis assumptions). Multivariate analyses were used to measure, explain and predict the relationship between B properties and pools in the composites. All statistical analyses were performed in R software using the agricolae, factoextra, FactoMineR, pvclust, corrplot, tideverse and nlstools packages [27].

The ATR-FTIR spectral signatures of the samples were used to generate and validate the PLS regression models and a total of 54 observations were used for the calibration and generation of the PLS mathematical models. In contrast, 13 samples (20%) were used for independent random external validation. The models were evaluated by analyzing the square root of the mean calibration error ($RMSE_{cal}$), coefficient of determination (R^2) and coefficient of calibration (R^2_{cal}). The model was cross-validated, using cross-validation RMSE ($RMSE_{cv}$), y-randomization RMSE ($RMSE_{y\text{-}rand}$), cross-validation R^2 (R^2_{cv}) and y-randomization R^2 ($R^2_{y\text{-}rand}$). The number of latent variables was determined by the lowest $RMSE_{cv}$ value of the 54 observations used for validation and used to calculate RMSE ($RMSE_{pred}$) (Eq. 8) and R^2 (Eq. 9) prediction (R^2_{pred}) [28]. Other validation parameters, such as R^2 between experimental and predicted values for the test dataset (r^2_m) and R^2 of randomization prediction y (r^2_p) were calculated based on the equations (Eqs. 10 and 11) [29]. The graphic images of the FTIR were obtained using the Origin Pro 8.5 software (OriginLab Co., Northampton, USA).

$$\mathrm{RMSE} = \sqrt{\frac{\sum_{i=1}^{n}\left(yi - \hat{Y}i\right)^2}{n}}. \tag{7}$$

$$R^2 = 1 - \frac{\sum_{i=1}^{n}\left(yi - \hat{Y}i\right)^2}{\sum_{i=1}^{n}\left(yi - \overline{Y}i\right)^2}. \tag{8}$$

$$r_m^2 = R^2\left[1 - \left(R^2 - R_0^2\right)^{\frac{1}{2}}\right]. \tag{9}$$

$$r_p^2 = R_{\mathrm{cal}}^2\left(R_{\mathrm{cal}}^2 - R_{\mathrm{y-rand}}^2\right)^{\frac{1}{2}}. \tag{10}$$

The dataset of B release kinetics in 2% citric acid—CA% was adjusted for different nonlinear mathematical models as an output of the relationship between the incubation time versus the amount of B released from

each nutrient source. The following mathematical models were fitted to the kinetics B dataset: Elovich model (Eq. 11), simple exponential model (Eq. 12), power function (Eq. 13) and hyperbolic model (Eq. 14).

$$\mathrm{Nt} = a + blnt \tag{11}$$

$$\mathrm{Nt} = N0\left(1 - e^{-kt}\right) \tag{12}$$

$$\mathrm{Nt} = a \times b^{t} \tag{13}$$

$$\mathrm{Nt} = \frac{N0 \times t}{(N0 \times b + t)} \tag{14}$$

where Nt = fraction of B released at the evaluated time; a = initial content of B released; b = B released at a constant rate; t = release time (hour); N0 = maximum amount of B released during the kinetic study. The best model was selected based on the highest coefficient of determination (R^2), the lowest value of the root mean square of error (RMSE) and the lowest value of the Akaike information criterion (AIC) [30]. Principal component analysis (PCA) was performed to evaluate the relationship between the properties of the composites produced in this study.

Results and discussion

Chemical properties of biochar and composites

Research demonstrated that there were distinct variations in biochar characteristics influenced by feedstock type and pyrolysis temperature (Table 3). Elevated temperatures generally increased biochar pH, ash content and fixed carbon (FC), enhancing the potential for soil amendment and C sequestration. Notably, the electrical conductivity (EC) of biochar decreased in BSC' feedstock due to the formation of stable inorganic compounds at higher temperatures. Additionally, while higher temperatures reduced biochar yield and volatile matter across all feedstocks, the loss of C and N was particularly pronounced in FSC due to its higher susceptibility to thermal degradation. This phenomenon can be attributed to the composition of FSC, which is mainly amino acids and proteins and is prone to degradation at higher temperatures due to the higher N content [31]. The temperature rise led to a decrease in VM, implying an increase in the concentration of inorganic elements in the pyrolyzed materials [32], due to the progressive loss of acidic surface functional groups, primarily aliphatic carboxylic acids [33]. This caused an increase in pH and aromatic character of the carbonized matrices at 550 °C [34]. However, the extent of this pH increase was found to be dependent on the pyrolyzed feedstock, as reported in other studies for FCM [35], FSC [36] and FSS [15].

There was an increase in EC with the rise of pyrolysis temperatures owing to the optimization of conductive properties possibly due to the greater presence of more soluble salts [33], except for BSC', which reduced EC with the intensification of the carbonization process. Additionally, an increase in pyrolysis temperature led to a reduction in biochar yield, VM and C and N contents across all biochars. These changes are attributed to enhanced thermal degradation, chemical transformations and volatilization of organic compounds from the feedstocks at higher temperatures [37]. The ash and FC content relatively increased with pyrolysis temperatures, possibly due to the accumulation and formation of compounds such as hydroxide and carbonate, which elevate the FC [38] and the pH values for most biochars [37].

Our study investigated the impact of B sources, feedstock types and pyrolysis temperatures on biochar properties, as detailed in Table 4. The incorporation of B into biochars, specifically in the form of BA, led to a reduction in acidification across several samples (CCM-BA,

Table 3 Biochar properties as influenced by feedstock

Biochar	pH	EC	Yield	VM	Ash	FC	Elemental composition		C:N ratio
		(dS m^{-1})	(%)				(%)		
							C	N	C: N
BCM	9.1	6.4	69	57	52	9.3	35	2.1	16.6
BCM'	10.7	8.2	53	56	60	11.1	26	1.9	13.1
BSC	9.2	7.3	81	72	32	3.9	41	6.5	6.4
BSC'	10.4	2.9	60	53	60	12.5	25	2.4	10.7
BSS	6.2	1.3	88	34	71	4.8	16	2.1	7.6
BSS'	7.1	1.5	69	28	78	5.4	12	1.2	10.3

Values are mean ± standard deviation (n = 3), except yield (%) (n = 1); EC: electrical conductivity; VM: volatile matter; Ashes; FC: fixed carbon; C: carbon; N: nitrogen; C/N: carbon/nitrogen ratio. BCM: chicken manure biochar at 300 °C; BCM': chicken manure biochar at 550 °C; BSC: shrimp shell biochar at 300 °C; BSC': shrimp shell biochar at 550 °C; BSS: sewage sludge biochar at 300 °C; BSS': sewage sludge biochar at 550 °C

Table 4 Basic characterization of the composites

Composite	pH	EC	Yield	VM	Ashes	FC	Elemental composition		C:N ratio
		(dS m^{-1})	(%)				(%)		
							C	N	C:N
CCM-BA	6.6 ± 0.1	9.0 ± 0.0	70	45 ± 0.0	47 ± 0.0	6.0 ± 0.0	19.9 ± 0.1	3.6 ± 0.0	5.6
CCM-BA'	7.7 ± 0.0	9.6 ± 0.0	55	37 ± 0.0	35 ± 0.0	24.0 ± 0.0	20.2 ± 0.1	1.9 ± 0.0	10.7
CCM-BX	9.3 ± 0.0	16.3 ± 0.0	72	54 ± 0.0	43 ± 0.0	1.4 ± 0.0	21.6 ± 0.1	3.4 ± 0.0	6.3
CCM-BX'	9.3 ± 0.1	16.0 ± 0.0	53	38 ± 0.0	28 ± 0.0	33.0 ± 0.0	19.5 ± 0.1	1.5 ± 0.0	13.4
CSC-BA	7.1 ± 0.0	9.0 ± 0.0	72	52 ± 0.0	40 ± 0.0	5.8 ± 0.0	21.1 ± 0.1	5.3 ± 0.0	3.9
CSC-BA'	7.6 ± 0.1	5.6 ± 0.0	48	60 ± 0.0	22 ± 0.0	18.0 ± 0.0	16.5 ± 0.1	2.6 ± 0.0	6.4
CSC-BX	9.2 ± 0.0	14.9 ± 0.0	70	52 ± 0.0	41 ± 0.0	3.7 ± 0.0	18.2 ± 0.1	2.6 ± 0.0	6.9
CSC-BX'	9.7 ± 0.0	11.0 ± 0.0	47	30 ± 0.0	26 ± 0.0	42.0 ± 0.0	16.7 ± 0.0	2.2 ± 0.0	7.5
CSS-BA	5.8 ± 0.0	3.2 ± 0.0	75	39 ± 0.0	38 ± 0.0	20.0 ± 0.0	9.7 ± 0.1	3.4 ± 0.0	2.8
CSS-BA'	6.3 ± 0.1	1.30 ± 0.0	62	36 ± 0.0	15 ± 0.0	49.0 ± 0.0	8.7 ± 0.0	1.0 ± 0.0	8.3
CSS-BX	9.2 ± 0.0	14.0 ± 0.0	77	13 ± 0.0	37 ± 0.0	53.0 ± 0.0	12.1 ± 0.1	1.7 ± 0.0	6.9
CSS-BX'	9.1 ± 0.0	8.5 ± 0.0	63	21 ± 0.0	12 ± 0.0	66.0 ± 0.0	9.7 ± 0.0	1.0 ± 0.0	9.9

Values are mean ± standard deviation ($n = 3$), except yield (%) ($n = 1$); VM: volatile matter; Ashes; FC: fixed carbon; C: carbon; N: nitrogen; C/N: carbon/nitrogen ratio. Composites: CCM-BA: chicken manure + boric acid at 300 °C; CCM-BX: chicken manure + borax at 300 °C; CCM-BA': chicken manure + boric acid at 550 °C; CCM-BX': chicken manure + borax at 550 °C; CSC-BA: shrimp waste + boric acid at 300 °C; CSC-BX: shrimp carcass + borax at 300 °C; CSC-BA': shrimp carcass + boric acid at 550 °C; CSC-BX': shrimp carcass + borax at 300 °C; CSS-BA: sewage sludge + boric acid at 300 °C; CSS-BX: sewage sludge + borax at 300 °C; CSS-BA': sewage sludge + boric acid at 550 °C; CS-BX': sewage sludge + borax at 550 °C

CCM-BA', CSC-BA, CSC-BA', CSS-BA, CSS-BA'), with decrease values ranging from 6.4% to 28.0% compared to controls. This reduction is linked to the swift removal of organic compounds and the introduction of basic cations. Elevated pyrolysis temperatures increased the pH in certain BA-doped samples (CCM-BA', CSC-BA', CSS-BA'), with increase values between 7.0% and 16.7%.

Conversely, BX-doped biochars (CCM-BX', CSC-BX') exhibited pH reductions of 13.1% and 6.7%, respectively. In contrast, CCM-BX, CSS-BX and CSS-BX' samples showed pH increase, indicating a shift towards alkaline conditions. The increased values were 2.2%, 48.4% and 28.2%, respectively, with CSC-BX remaining stable. High pyrolysis temperatures slightly increased CSC-BX' pH by 5.4%, while CSS-BX' had a 1.1% decrease. The introduction of B significantly influences the thermal decomposition of biochars, affecting the functional group composition from feedstocks and the acid–base equilibrium of the end product. These alterations impact the characteristics and stability of the biochar composites.

Investigating the catalytic effects of B-doped biochar during pyrolysis uncovers significant pH alterations and the creation of active chemical sites within the carbonized structures, as demonstrated by Chen et al. [39]. The atomic radius similarity between B and C leads to unique structural interactions that are pivotal for enhancing the biochar composites' physicochemical attributes, a concept further detailed by Kim et al. [40]. BA application typically maintains the composite pH near neutrality due to its weak acid nature and is prone to donating H^+ ions. In contrast, BX shifts the environment towards alkalinity by releasing borate ions and elevating the OH^- ion concentration in the synthesis medium, corroborating other findings [41]. Such variations in pH modulation are crucial, given the influence of active sites on the composites' physicochemical transformations [42]. Other researchers [43] point out that the distinct pH modulation effects of BA and BX underscore the nuanced impact of biochar-B properties. This emphasizes the criticality of choosing appropriate B sources for targeted environmental applications, offering a comprehensive perspective on their role in enhancing soil health and environmental sustainability.

While conducting this research, we observed a general trend where higher pyrolysis temperatures increased the EC in all biochar composites except for the CSS-BA composite. This particular composite showed a 13.3% reduction in ash content compared to its non-B-doped counterpart. Conversely, the CCM-BA composite experienced a 6.7% increase in ash content relative to its biochar-B variant, indicating that pyrolysis temperatures generally boosts EC.

Contrastingly, BA composite EC diminished with rising pyrolysis temperatures, an effect that was not observed when BX was used for doping, potentially due to increased deprotonation of groups. This process likely facilitates a new electronic structural modulation

of the C matrix, as suggested by Chen et al. [39]. Supporting literature indicates that pH elevation leads to deprotonation, altering EC by enhancing the medium's conductivity through the introduction of charged ions [44]. This is significant because EC is directly influenced by charged ions, suggesting a more efficient electron conduction pathway.

Our analysis demonstrated a notable improvement in composite yields when B was incorporated into FCM C matrix composites. Specifically, B-doping at a pyrolysis temperature of 300 °C resulted in a 5.1% increase in yield with the BX-doping method, while at 550 °C, BA-doping led to a 4.4% increase. Conversely, the beneficial effects of B-doping were not evident in biochars from alternative feedstocks, where yields declined regardless of the doping method. Minimal impact on yields was observed from B-doping in feedstock-B mixtures. What is noteworthy is that the composites CCM-BX, CSC-BA and CSS-BX recorded the highest average yields of 72.5%, 71.8% and 77.3%, respectively. This suggests that B acts as a potent chemical activator in the carbonization process, promoting the development of a more favorable pore structure within the biochar, thereby enhancing yield. Our findings align with those of Zhang et al. [5], who also identified B sources as advantageous activators for biochar yield enhancement.

The VM content in CSC-BA', CSS-BA and CSS-BA' composites was increased by 13.7%, 14.7% and 28.8%, respectively, compared to their unmodified biochar counterparts, reaching levels of 60%, 39% and 36%. Typically, the VM content decreases as the pyrolysis temperature increases. However, an unexpected rise in VM by 15% and 68.5% for CSC-BA' and CSS-BX', respectively, from 300 °C to 550 °C, indicates more intense pyrolysis conditions. This suggests that B-doped biochars might follow unique thermal decomposition pathways, increasing VM production at higher temperatures.

Furthermore, while VM preservation usually increases with pyrolysis temperatures, reducing the emissions of volatile gases and liquids, CSC-BA' and CSS-BA' showed an increase in VM. This increase could be due to the preferential loss of less stable molecular oxygen (O), while more stable B structures remain [45]. Additionally, an increase in aromaticity, associated with higher losses, reduces substance volatility. This process results in a more stable and less volatile composition, potentially offering benefits for using B to improve catalytic activity [45] and proposing a non-radical degradation pathway based on direct electron transfer, especially for FSC and FSS matrices.

Composites CCM-BA, CSC-BA and CSS-BA, produced at 300 °C, exhibited the highest ash contents, with 47%, 40.1% and 38.5%, respectively. These contents decreased as the temperature increased, showing an inverse relationship between temperature and ash content. This phenomenon contrasts with the increases in ash content observed in another feedstock-derived biochar (CSC-BA and CSC-BX), which were 26.5% and 30.3%, respectively. This underscores the significant impact of the property of sugarcane FSC feedstock, enriched with minerals such as Ca, P and Mg, which show greater resistance to volatilization during pyrolysis [46].

The unique mineral composition of FSC feedstock is crucial for the varied ash content outcomes following pyrolysis. Due to their thermal stability, these minerals tend to accumulate in higher concentrations after pyrolysis at elevated temperatures [47]. Specifically, calcium carbonate ($CaCO_3$) present in FSC decomposes into calcium oxide (CaO) and carbon dioxide (CO_2) during the process, with CaO contributing significantly to the high ash content of the biochar. In contrast, CO_2 is volatilized [48]. Additionally, the thermal degradation of chitin found in FSC results in an ash-rich residue due to its N and mineral content [48]. These variations in ash content, especially the notable increases in CSC-BA and CSC-BX, highlight the influence of feedstock composition on pyrolysis and the resulting characteristics.

The incorporation of BX into the FSS matrix significantly catalyzed an increase in FC content, achieving a rise of over 1000% when compared to traditional biochars. This notable enhancement was especially evident in the CCM-BX' and CSC-BX' composites at higher temperatures. The relationship between pyrolysis temperatures and the FC content is strongly positive, highlighting the effectiveness of C preservation within the matrix. This relationship indicates that at higher temperatures, C forms more robust bonds with the matrix, which enhances stability. This effect is crucial for the functionality of BA-based composites for thermal stability [5], where B atoms substitute C atoms. This substitution is facilitated by the similarity in their atomic radii and the integration of B into the C sp^2 network [49], thereby enhancing structural integrity and C preservation during pyrolysis, boosting the FC content. Additionally, this finding paves the way for optimizing C structuring at various scales, including morphology, crystalline parameters and the B-doping environment [50], underlining the materials' versatility and efficacy in C preservation.

At the pyrolysis temperature of 550 °C there was a decrease in the total N content in the biochar (Table 3). However, BA-containing composites, specifically CCM-BA, CSC-BA and CSS-BA, exhibited N preservation, with increases of 71%, 8.3% and 62%, respectively, compared to pristine biochars. This preservation can be attributed to the ability of B to act as a stabilizing agent for N. B forms complexes with nitrogen molecules,

reducing volatilization during pyrolysis due to the interaction between the empty p orbital of B and the partially filled p of elements such as N and O [51].

On the other hand, adding BX reduced N content, except for CCM-BX, which recorded an increase of 62%. High-temperature treatment at 550 °C with BX-doping resulted in composites with a high C/N ratio, notably in CCM-BX (13.4), CSC-BX (7.5) and CSS-BX (9.9), when compared to pristine biochars. BA-doping led to lower C/N ratios, suggesting that the association of N content with the porous structure of the biochar helps preserve N during pyrolysis or minimizes the loss of nutrients to the gas phase during carbonization. Conversely, compositions that exhibited decreased ash, C and N content indicated that the residues were more readily volatilized or converted into gases, thereby diminishing B levels in alkaline composites due to reduced polymerization. Consequently, this leads to a less condensed C structure that is more vulnerable to thermal degradation [46].

The FSC feedstock is rich in proteins, chitin and N, which decompose during pyrolysis, potentially releasing N as ammonia (NH_3) or incorporating it into the biochar structure, enhancing the adsorption and retention of nitrogenous functional groups. The presence of BA-doping revealed a chemical bonding between B and N, forming amino-borane complexes and the interaction of nucleophilic sites in amides with boranes, creating thermally stable bonds [52]. This stability is influenced by the electronic value [52] of B-substituted groups, reducing the likelihood of decomposition and preserving the content within the matrix.

This research demonstrated that the behavior of B in doped materials significantly varies based on the feedstock type and the doping agent used, as well as the pyrolysis temperatures employed. It was noted that CCM-BA showed a 16.8% reduction in B content. The FCM, being rich in volatile organic compounds, suggests that chemical reactions or thermal decomposition of certain manure components may affect B retention, attributing to the higher volatility of BA at elevated temperatures which facilitates B loss during pyrolysis. Conversely, CSC-BA (138 g kg^{-1}) and CSS-BA (146 g kg^{-1}) exhibited increases in B content of 3.4% and 14.4%, respectively (Table 5). This phenomenon could be explained by the formation of more stable structures that incorporate B, possibly due to the interaction of BA with specific components such as chitin and various organic and inorganic compounds, which may form structures that encapsulate B, preventing its volatilization and potentially forming stable B-organic compounds at high temperatures.

Both CCM-BX and CCM-BX' maintained stable B levels when doped with BX. BX, being a thermally more stable B compound than BA, tends to integrate into the matrix more efficiently, preventing loss during pyrolysis. In contrast, CSC-BX and CSS-BX showed decreases of 19.4% and 4.4%, respectively, while CCM-BX' displayed thermal stability differing from the other composites.

Table 5 Boron pools in biochar-based composites

Boron (B)							
Composite	**W**	**T**	**NAC**	**CA%**	**W Index**	**NAC Index**	**CA% Index**
	(g kg^{-1})				**(%)**		
CCM-BA	1.6 ± 0.1	166.7 ± 0.1	101.5 ± 4.9	80.9 ± 0.2	0.9 ± 0.1	60.9 ± 2.9	48.5 ± 0.1
CCM-BX	0.9 ± 0.1	75.6 ± 0.1	53.2 ± 1.9	70.7 ± 0.3	1.2 ± 0.1	70.5 ± 2.6	93.6 ± 0.4
CCM-BA'	2.1 ± 0.1	138.7 ± 0.1	100.0 ± 3.1	86.6 ± 6.3	1.5 ± 0.1	72.1 ± 2.2	62.4 ± 4.6
CCM-BX'	1.0 ± 0.1	75.5 ± 0.1	55.5 ± 0.8	56.3 ± 4.0	1.4 ± 0.1	73.5 ± 1.0	74.5 ± 5.4
CSC-BA	2.4 ± 0.1	133.2 ± 0.1	125.9 ± 4.8	90.0 ± 1.1	1.8 ± 0.1	94.5 ± 3.6	68.2 ± 0.8
CSC-BX	1.6 ± 0.1	91.3 ± 0.1	88.3 ± 0.8	89.8 ± 1.0	1.8 ± 0.1	96.8 ± 0.9	98.4 ± 1.2
CSC-BA'	2.6 ± 0.1	137.7 ± 0.1	132.5 ± 1.9	83.5 ± 3.1	1.9 ± 0.1	96.2 ± 1.3	60.7 ± 2.3
CSC-BX'	1.6 ± 0.1	73.6 ± 0.1	70.8 ± 0.7	56.3 ± 0.1	2.2 ± 0.1	96.2 ± 0.7	61.7 ± 0.2
CSS-BA	2.2 ± 0.1	127.5 ± 0.1	114.9 ± 3.1	83.2 ± 6.4	1.7 ± 0.1	90.1 ± 2.5	65.2 ± 5.0
CSS-BX	1.1 ± 0.1	66.2 ± 0.1	57.0 ± 0.9	50.0 ± 1.0	1.7 ± 0.1	86.0 ± 1.3	75.5 ± 1.5
CSS-BA'	2.0 ± 0.1	145.8 ± 0.1	113.6 ± 2.6	64.1 ± 5.8	1.3 ± 0.1	77.9 ± 1.8	44.0 ± 3.9
CSS-BX'	1.1 ± 0.1	63.3 ± 0.1	61.2 ± 1.0	35.8 ± 0.3	1.8 ± 0.1	96.8 ± 1.6	56.6 ± 0.4

Values are mean ($n = 3$); B in H_2O was determined ± 0.01 in a solution of H_2O at a ratio of 1:10 (w/v); content of soluble B in total (T) was determined by total digestion of the composites; B in neutral ammonium citrate water (NAC); B in content of B soluble in citric acid at 2% (CA%); H_2O Index, NAC Index and CA% Index represent the B content in relation to the extractors and the total B content. Composites: CCM-BA: chicken manure + boric acid at 300 °C; CCM-BX: chicken manure + borax at 300 °C; CCM-BA': chicken manure + boric acid at 550 °C; CCM-BX': chicken manure + borax at 550 °C; CSC-BA: shrimp waste + boric acid at 300 °C; CSC-BX: shrimp carcass + borax at 300 °C; CSC-BA': shrimp carcass + boric acid at 550 °C; CSC-BX': shrimp carcass + borax at 300 °C; CSS-BA: sewage sludge + boric acid at 300 °C; CSS-BX: sewage sludge + borax at 300 °C; CSS-BA': sewage sludge + boric acid at 550 °C; CS-BX': sewage sludge + borax at 550 °C

These results suggest that although BX forms stable structures with some organic components, it may not interact as effectively with substances in these other feedstocks; otherwise, these substances may facilitate the degradation of BX at higher temperatures.

Furthermore, the increase in total B content with rising pyrolysis temperatures in BA-doped composites, which enhances the microstructure and improves oxidation resistance, aligns with the observations of Smith et al. [53], who noted improved nutrient stabilization in biochar under high thermal conditions. However, the reduction in total B content in BX-doped composites at higher temperatures highlights the complex interactions during pyrolysis that may involve decomposition and chemical transformations [54], potentially affecting how B is incorporated into biochar [55]. The observed volatilization of B at elevated temperatures reflects the findings of Jones et al. [54], who documented the susceptibility of certain B compounds to thermal degradation, thereby reducing the amount of B retained in biochar and impacting its stability.

Water solubility assessments showed that CSC-BA and CSC-BA' composites have higher immediate B availability, making them particularly effective for soil applications. The enhanced total B content due to BA-doping suggests that these composites could offer prolonged B supplementation. The solubility and availability metrics, specifically NAC and CA%, indicate that CSC-BA and CSC-BA' are well-suited for agricultural applications, with CSC-BX demonstrating an impressive CA% of 98.4%, showcasing its effectiveness in B solubility and its potential to facilitate B distribution in acidic soils.

The water solubility of B in the CSC-BA and CSC-BA' composites suggests they can provide immediate B availability to plants, which aligns with the findings of Shireen et al. [56], who emphasized the importance of micronutrient accessibility for plant health. The rapid solubility of B in these composites indicates their utility in quickly addressing B deficiencies in agricultural settings, potentially enhancing soil fertility and crop yield.

The significant CA% index observed in the BX composites suggests their capacity to interact with metal ions, enhancing the solubility of these metals through the formation of chelated complexes. This is in line with another paper [57], which emphasized the role of biochar composition and modification in effective dye degradation. Meanwhile, the NAC index observed in the BA composites indicates that these composites can form soluble complexes under neutral pH conditions without necessarily undergoing an acidification reaction [58].

Infrared spectroscopy

The detection of hydroxyl groups (–OH) with peaks spanning 3.100 to 3.500 cm^{-1} indicates the presence of carboxyl, phenols, alcohols and water (Fig. 1). This range suggests possible changes in amide compounds, such as dehydration or decomposition, illustrated in Fig. 1a, c. The retention of hydroxyl groups and the distinct peak linked to the B-O/B-C bond, as shown in Fig. 1a, b, indicate the effective integration of B atoms into the pyrolyzed matrix. This integration not only enhances the composite's physicochemical properties but also contributes to increased B solubility in water, as observed by Zhang et al. [15].

The observation of CH aliphatic stretching vibrations between 2.920 and 2.885 cm^{-1}, alongside a specific vibration at 2.351 cm^{-1} indicating C–CO_2 stretching, validates the presence of porous structures with significant graphitization. This observation, indicating disordered defects, is further confirmed by characteristic CH stretching peaks at 3220 cm^{-1} in CSC-BA' and CSS-BA', and by our SEM findings [59].

An intensified band near 1600 cm^{-1} points to the presence of aromatic (C=C, C=N), ketonic/aldehydic (C=O) and steric (–COO) vibrations, according to Ateş et al. [60], crucial for the composite's chemical characterization, as depicted in Fig. 1b, d. The B–C bond vibration observed at 1020 cm^{-1} aligns with previous research [61], highlighting the significance of infrared vibrations associated with B–C bonds. This suggests that a meaningful interaction occurs in these groups within the composites' structures and confirms the origin of the aromatic C=C bond at 1430 cm^{-1}, essential for understanding the physicochemical transformations triggered by functional group modifications at the lower pyrolysis temperature of 300 °C.

Notably, amide groups are distinguishable in the 1650–1700 cm^{-1} range, as detailed in Fig. 1c. Moreover, Zhou et al. [62] emphasized the enhancement in performance and stabilization of B when associated with N-containing borate ester groups, facilitated by the lone electron pairs on N that complex B empty 2*p* orbit. This interaction, revealing a substantial presence of B and N elements (Table 3), demonstrates the functional groups' superior activity in BA-doped composites at both 300 °C and 550 °C.

Signals around 1435 cm^{-1} might indicate carbonyls or carbonates, with stretching in carboxylic acids between 1319 and 1232 cm^{-1}, especially notable in composites produced at 300 °C. The B-doped C-rich materials exhibit configurations in both the graphitized and surface edge regions, more so with BA-doping at 550 °C. This outcome, likely due to carbonyl-like groups (C=O) that

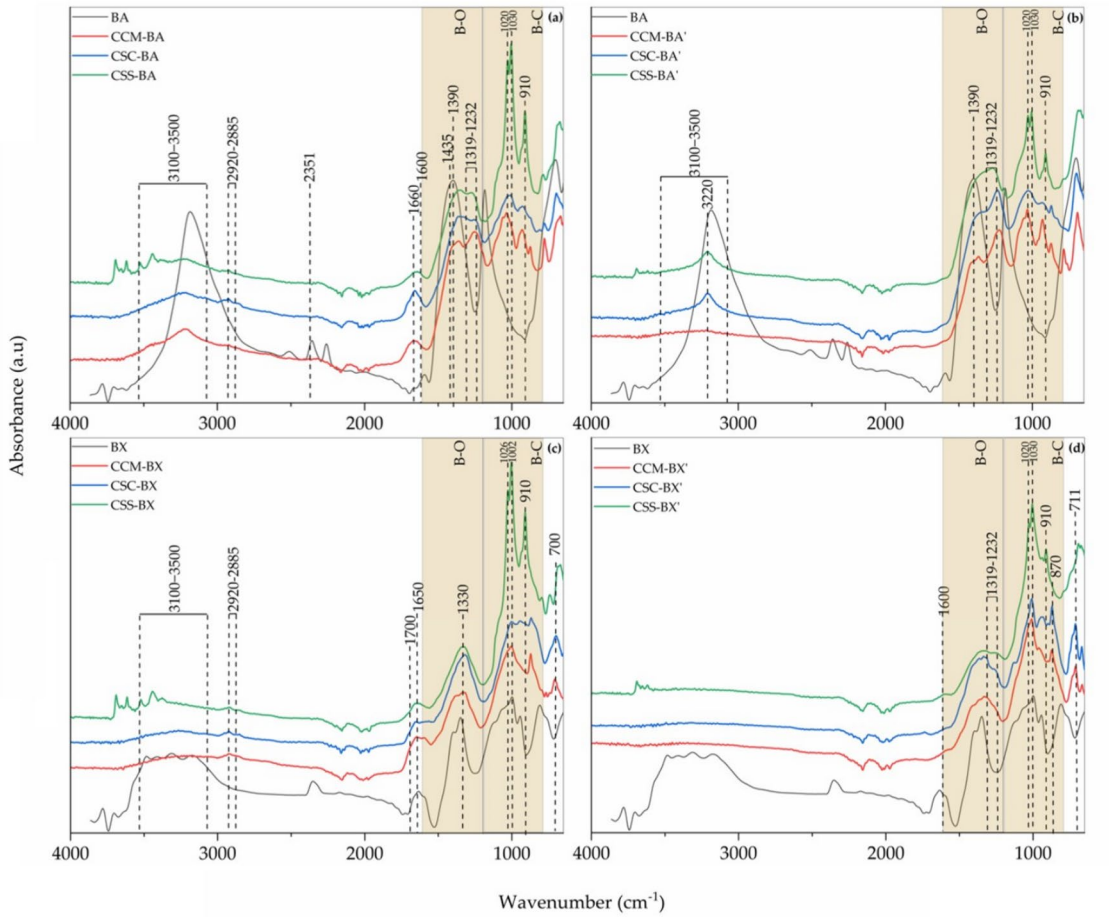

Fig. 1 Fourier transform infrared spectroscopy (FTIR) and the main peaks and characteristics of the chemical groups found in composites produced from biochar doped or not with boric acid or borax. **a** composites doped with boric acid at 300 °C; **b** composites doped with boric acid at 550 °C; **c** Composites doped with borax at 300 °C and (**d**) composites doped with borax at 550 °C

form C–O–B type bonds and groups, alongside carboxylic acids (–COO), suggests enhanced oxygen activation compared to BX-doping, which displays less interaction with C under pyrolysis [63].

The role of B in O activation, improving surface charge distribution and inducing polarization, is well documented [64, 65] and leads to the formation of acidic functional groups. Conversely, BX-doping tends to make the composites more alkaline by introducing unpolarized basic groups. The presence of B–O and B–O–B bonds around 1390 cm^{-1}, indicative of B incorporation via borates or esters, is particularly prominent in composites processed at 300 °C. This enhances interactions with certain feedstocks, improving the composite's chemical properties like acidity and polarity, as elaborated in Fig. 1b [66] and highlighted by recent findings that highlight the importance of these bonds in biochar activation with BA.

Spectral analysis within 800–1200 cm^{-1} and 1200–1600 cm^{-1} showcases interactions of B–C and B–O groups, respectively, without evidence of B-B bonds. Changes in the 1180–950 and 950–750 cm^{-1} regions hint at P–O–B bonding in BX-doped samples, with significant shifts observed for pyrolysis temperature changes, as shown by the absorption peaks at 3419 cm^{-1} for (–OH) in BX-doped composites produced at 300 °C and water stretching vibration deformation around 1330 cm^{-1} with temperature increase, as illustrated in Fig. 1c, d. Considering this relationship, using BA with its B–A symmetric stretch should yield an active peak at around 1200–1600 cm^{-1}, while BX has a broad band of asymmetric stretching with a peak around 800–1000 cm^{-1} [67].

Principal Component Analysis (PCA) and cluster analysis revealed significant effects on the composites, indicating that B is incorporated into the matrix

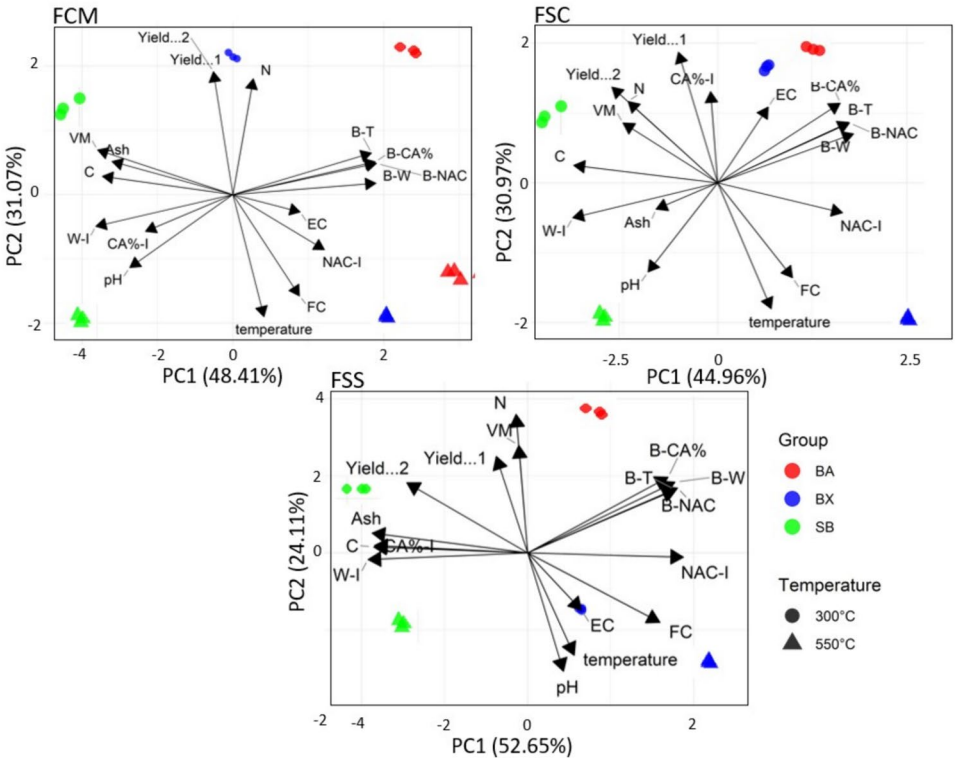

Fig. 2 Principal component analysis (PCA) of compounds produced in relation to the absence or source of B

via borate ester bonds (Fig. 2). Variations in the water solubility of B across different composites displayed unique patterns influenced by the doping material used. In composites extracted by neutral ammonium citrate (B-NAC), an increase in B solubility was noted, whereas those doped with BX showed reduced solubility. This variation is further highlighted by an observed inverse relationship between solubility and other composite properties, such as pH, VM, ash content and C content.

For the CSC-BA there was an increased availability and solubility of B, especially when in the NAC form. This interaction aligns well with the composites' properties such as N, VM, FC and EC (Tables 3 and 4). Additionally, doping with BX modified the solubility of B-CA% at 300 °C and enhanced the solubility of B-NAC at 550 °C. These changes in solubility were associated with shifts in electrical conductivity and ash content, ultimately leading to a decrease in the total B content within the composite.

CA%, acting as a mimic of natural root exudates, proved effective in enhancing B release, especially in the CCM-BX, CCM-BX' and CSC-BX composites under alkaline pH conditions that favor the solubilization of borate ions. The presence of CA% facilitated the formation of soluble B complexes with metal ions, thereby enhancing B bioavailability. These alkaline conditions also led to an increase in ash content and the C/N ratio, which helped stabilize B within the composite. This stabilization was further supported by the promotion of BO functional group formation, alongside an increase in the content of B and N [62].

The CSS-BA doping was found to promote clustering of B solubility in NAC, linked to VM. There was an increase in the VM content and N preservation in CSC-BA', consequently increasing the VM and B levels. The spectral feature retention at 3220 cm^{-1}, associated with a bend around 1630 cm^{-1} as observed in CSS-BA' samples, might be due to the preservation of hydroxyl groups even at raised pyrolysis temperatures. These findings suggest that specific functional groups such as C–OH and B–OH found at 3446 cm^{-1} and 3220 cm^{-1} are conserved while reducing the B–C bonding at 1020 cm^{-1}. This change corresponds to the presence of monocrystalline B carbide in covalent organic structures and amorphous B carbide, crucial for composites' structural integrity [68]. In conclusion, the PCA provided valuable insight regarding the physicochemical dynamics of B incorporation into different matrices. These findings showcase the interaction between doping agents, pyrolysis temperature and matrix composition, collectively influencing the solubility and bioavailability of B in the resulting composites.

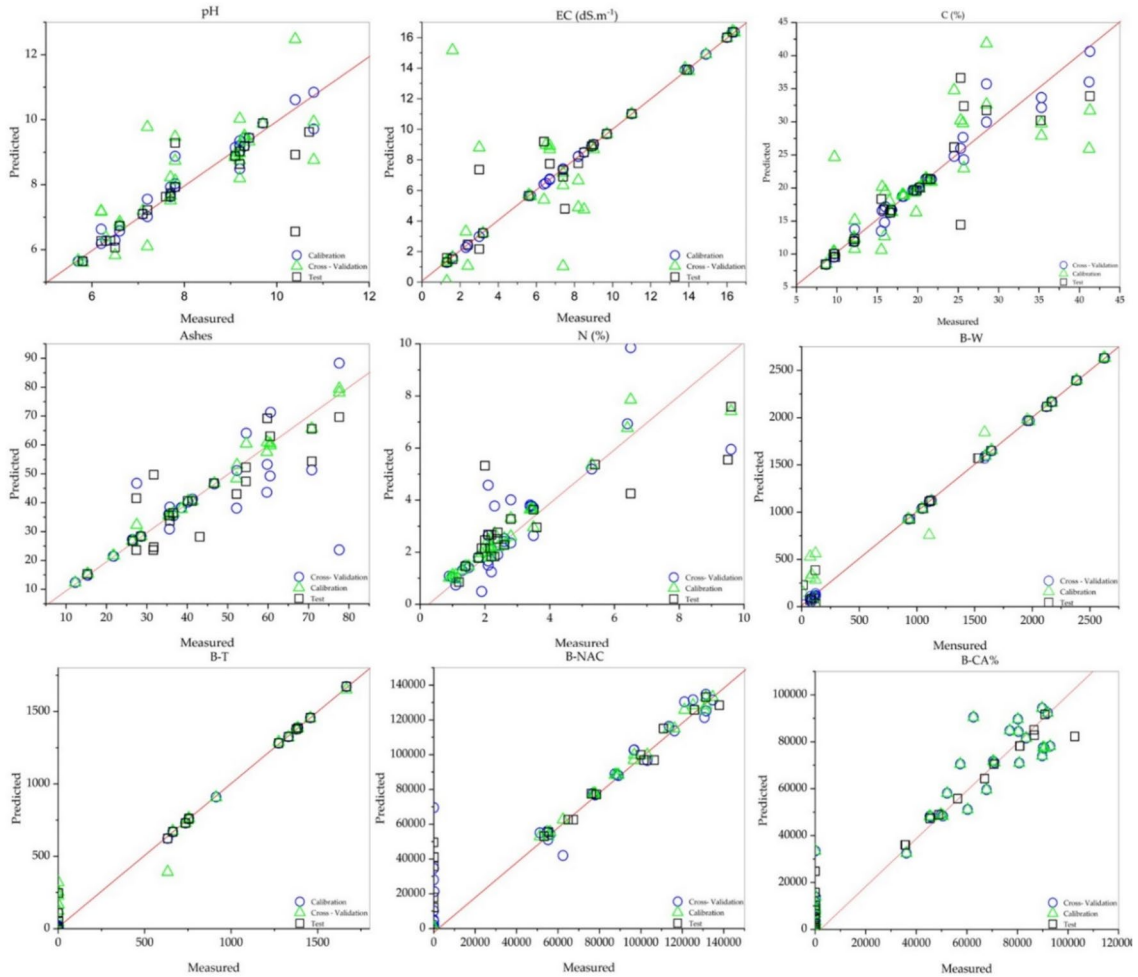

Fig. 3 PLS regression based on ATR-FTIR in order to predict the properties and nutrient pools found within the composites

Prediction capacity of PLS models

Modeling through FTIR-PLS proved to be far superior when forecasting specific properties, highlighting the efficacy of the suggested approach for accurately determining key characteristics. Traditionally, this process has involved significant manual effort and substantial consumption of laboratory resources (Table S2). In particular, the introduction of B into biochar derived from chicken manure, shrimp carcass and sewage sludge matrices led to composites exhibiting diverse nutrient profiles and a broad spectrum of chemical and physical–chemical traits. The models we developed, based on ATR-FTIR, were notably successful in predicting the B concentration within these composites, furnishing dependable estimates of their properties (Fig. 3).

The calibration phase for our PLS models revealed exceptionally high correlation coefficients (R^2), all surpassing 0.93, while in some instances, reaching an R^2 of 0.60, which is considered satisfactory according to Kiralj et al. [28]. This strength was also apparent in cross-validation phases, where R^2 values exceeded 0.81 alongside minimal RMSE, as supported by others [69]. Notably, y-randomization test results for R^2 values exceeded the 0.5 thresholds, except for B-NAC, which neared 0.49, still within the acceptable range as defined by Roy et al. [29]. The discrepancy between R^2 values for calibration and prediction in each PLS model was consistently less than 0.2, showing no overfitting, in line with the criteria set by Kiralj et al. [28]. Furthermore, employing FTIR-ATR spectrum database-based PLS models for pH prediction showcased R^2 calibration values of 0.73 and prediction values between 0.71 and 0.73, with calibration RMSE of 0.11 and prediction RMSE of 0.27, indicating an accuracy comparable to existing literature [70].

The application of near-infrared reflectance spectroscopy for quick analysis of manure composites yielded calibration and validation determination coefficients of 0.788 and 0.615, respectively, with associated standard

errors (SEE for pH being 0.48 and SEP 0.60), demonstrating the potential of this approach [7]. For EC specifically, calibration R^2 stood at 0.8704, with validation R^2 at 0.8953, complemented by SEE of 1.74 and SEP of 1.87, underlining the method's effectiveness [7].

The robustness of the technique in predicting C content was confirmed with a calibration R^2 of 0.9610 and validation R^2 of 0.9128, highlighting the model's accuracy (SEE of 16.46 and SEP of 26.34) [7]. The NIR spectrum model for predicting biochar ash content was reported to have a prediction of R^2 of 0.92 and a cross-validation RMSE of 0.26 [71], while another study using NIR spectroscopy for biochars processed at various temperatures obtained a calibration R^2 of 0.99, RMSEC of 0.3, cross-validation R^2 of 0.94 and cross-validation RMSE of 0.8 [72].

Lastly, infrared spectroscopy provided substantial predictive accuracy for N content in NPK minerals and organic mineral fertilizers (OMFs), with calibration and cross-validation of R^2 values of 0.98 and 0.97 and corresponding RMSEs of 1.91 g kg^{-1} and 2.00 g kg^{-1}, respectively [70]. Near-infrared reflectance spectroscopy for manure composites showcased calibration and cross-validation coefficients of 0.9874 and 0.9735, with an SEE of 1.61 and SEP of 3.96 [7].

Kinetics of B release

The B release kinetics from biochar composites synthesized at 300 °C and 550 °C were detailed and assessed through an FTIR spectroscopic approach (Fig. 4). The application of an Exponential model described the release over time, with the Elovich model better characterizing the release for specific composites, offering insight into the nutrient release patterns essential for optimizing fertilization processes.

At 300 °C, biochars exhibited distinct release behaviors, with CCM-BX showing a striking 100% B release between 2 and 4 h, suggesting high solubility and minimal organic matrix binding. The order of B release was recorded as CCM-BX > CSC-BA > CSC-BX > CSS-BA > CSS-BX > CCM-BA. This is indicative of the influence a B source holds on nutrient release in chicken manure-based composites. For CCM-BA, an initial rapid release was observed, reaching a 10% release within the first hour and stabilizing thereafter.

With an increase in pyrolysis temperature to 550 °C, the B release was generally rapid, potentially due to modifications in surface adsorption characteristics. For composites doped with BX, the CCM-BX' showed an impressive 100% B release within the 24–48-h range. The B release trend for 550 °C biochars was: CCM-BX' > CSC-BX' > CSS-BA' > CSC-BA' > CCM-BA'. The elevation of pyrolysis temperature contributed to an 11% increase in the release rate for CCM-BA, while CSC-BA showed no significant difference, and CSS-BA presented a 10% increase.

With an increase in pyrolysis temperature to 550 °C, B release was generally rapid, potentially due to modifications in surface adsorption characteristics. These results suggest that doping with B significantly influences the nutrient release in chicken manure-based composites. The presence of B–O bonds, evidenced by the spectra at

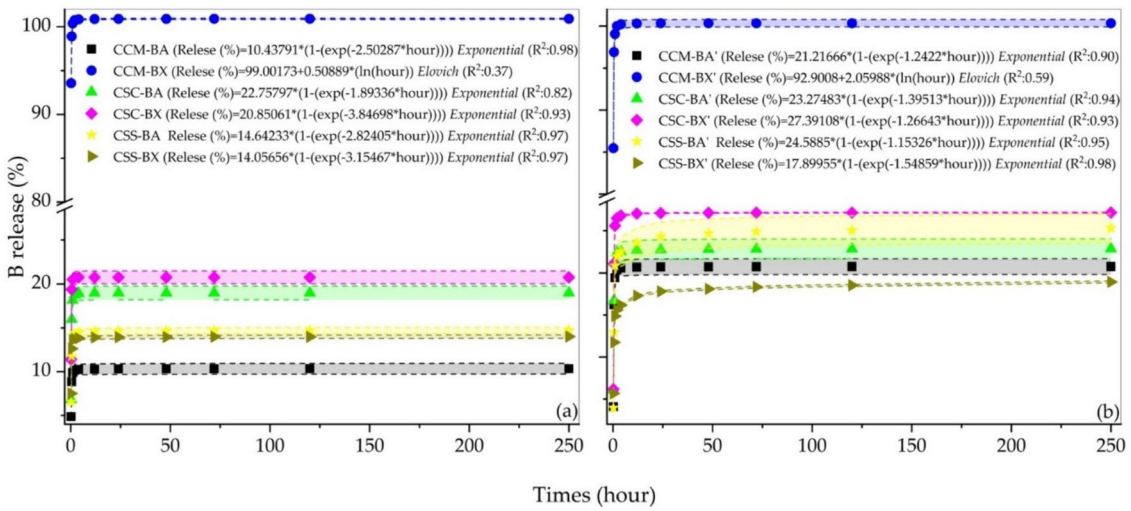

Fig. 4 Kinetics of B Release (B) as related to composites produced at 300 °C (**a**) and 550 °C (**b**) with the mixture of chicken manure, shrimp carcass and sewage sludge plus boric acid and borax prior to pyrolysis

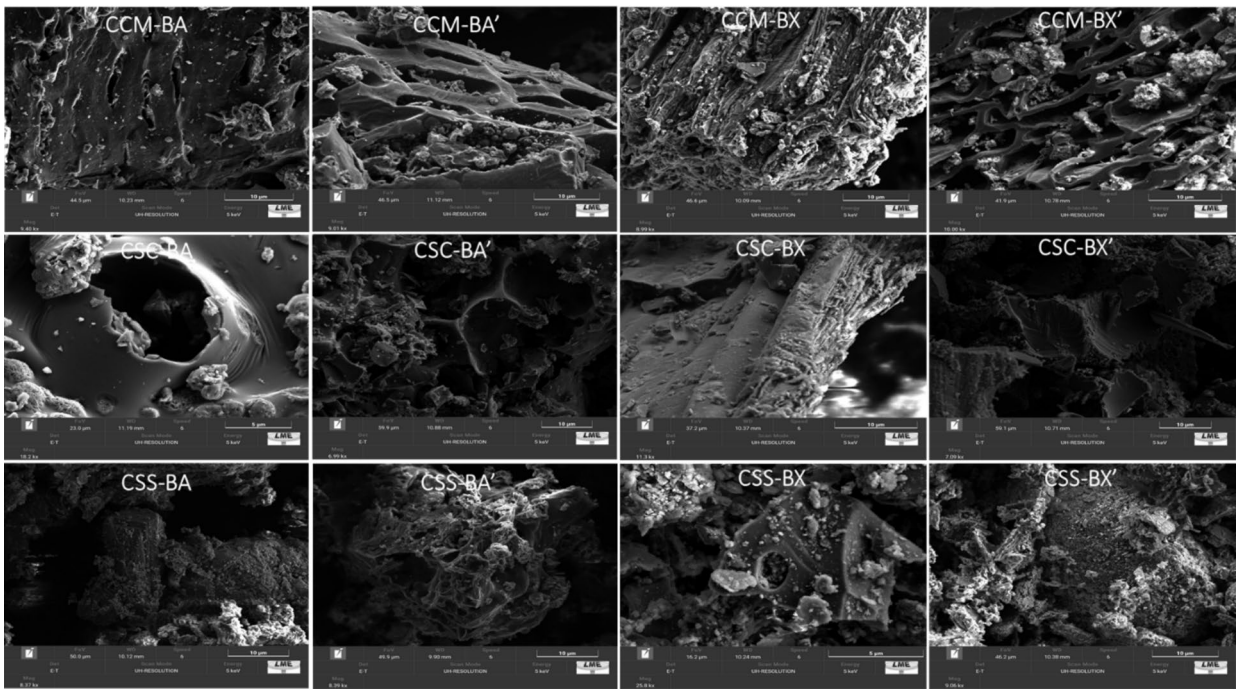

Fig. 5 Scanning microscopy obtained by FCM, FSC and FSS both under the influence of temperature 300 and 550 °C, as well as enriched with BA and BX. Magnified images at 10 µm

550 °C, indicates a greater interaction at this temperature [40, 73]. This interaction of B with organic compounds, whether through complexation or adsorption into the composites [74], contributes to the gradual release of B [75], which aligns with the patterns observed throughout our research (Fig. 5).

The doping also provides acidic Lewis sites and alters the electronic structure of the C matrix, enhancing the electron transfer rate and catalytic capacity, albeit influenced by thermal degradation [6]. This underscores the importance of carefully selecting the pyrolysis temperature to ensure the stability and functional efficacy of the biochar composites, as it modulates B release over time, which is crucial for sustainable agricultural practices.

Fourier transform infrared spectroscopy (FTIR)

SEM images depict variations in particle size and surface morphology among feedstocks, biochars, BA-based and BX-based (Fig. 4). BCM exhibits a heterogeneous, amorphous structure with a rough and porous surface, indicating diverse pore sizes and shapes. BCM' demonstrates structural loss and thermoplastic properties at 550 °C, leading to complete destruction during pyrolysis.

For CCM-BA, the SEM revealed elongated pores akin to channels, indicating a structure conducive to the release of gases and volatiles, aligning with the observed preferential release patterns. In contrast, the CCM-BA' sample, when subjected to higher temperatures, showed rounded pores, indicative of structural compromises such as pore collapse and overall matrix deterioration. CCM-BX biochars possessed shallow pores, consistent with a rapid 100% B release profile, whereas CCM-BX' displayed elongated but obstructed pores, potentially hindering the exchange of substances and ionic interactions, as confirmed by kinetic analyses.

CSC-BA biochar showed surface pores reminiscent of volcanic textures, augmenting pore orientation and connectivity, which likely contributed to a reduction in VM. Conversely, CSC-BA' was characterized by a highly porous structure with a hexagonal motif, while CSC-BX' retained a porous surface integrated with lamellar zones. The CSC-BX' variant, however, appeared massive and monolithic with a notable absence of discernible pores and cavities. The surface morphologies of both CSS-BA and CSS-BA' were rugged and porous, with high-temperature pyrolysis fostering the formation of surface precipitates. Similarly, CSS-BX and CSS-BX' biochars exhibited homogeneous surfaces as temperature escalated, lacking conspicuous porosity, and were peppered with opaque impurities owing to the synthesis of B compounds during pyrolysis [76].

Selected for greenhouse trials with Eucalyptus due to their substantial total B content, C, ash and VM, CSS-BA', CSC-BA and CSS-BX composites also demonstrated the

retention of functional groups associated with B complexation. The slow B release, as indicated in the kinetic study, places these composites as promising candidates for meeting the nutritional requirements of eucalyptus seedlings over different growth stages.

The SEM images captured in Fig. 5 illustrate the biochars and their composites, highlighting the morphological variances instrumental in B species implantation, as evidenced by the distinctive textural and structural characterizations when doped with BA and BX. The prominent peak attributed to C–B/B–O/C–O compounds [77] underscores the unique porosity and structural arrangement of CSC-BA (Fig. 1a), CSS-BA' (Fig. 1b) and CSS-BX (Fig. 1c). CSC-BA exhibits profound porosity akin to volcanic formations [60] and clearly defines the borate ester structure [42]. Simultaneously, CSS-BA' emphasizes surface precipitates with elevated pyrolysis temperatures and CSS-BX accentuates the valorization of compounds, maintaining structural integrity without noticeable porosity or cavities [60].

Agronomic efficiency of composites: nutrition and growth of eucalyptus

The results obtained in the cultivation of eucalyptus in Oxisols showed an increase in the production of shoot dry matter (SDM) when compared to the control without B addition (NB) (Fig. 6). The addition of composites not only increases the total dry matter (TDM) in comparison to plants treated only with B (BA p.a.), but also promotes a significant increase in root dry matter (RDM), which ensures an increase in vigor and establishment capacity of the seedlings, which is an important contribution to agricultural practices and eucalyptus cultivation management as described elsewhere [78].

The CSC-BA composite demonstrated a marked improvement over the BA treatment in enhancing dry matter production in eucalyptus grown in Oxisols. Specifically, in the RYL soil, there was an increase of 71.9% in Root Dry Mass (RDM), 106% in stem dry mass (SDM), and 96.9% in total dry mass (TDM). Similarly, in the DRL soil, the CSC-BA composite facilitated increases of 139% in RDM, 99.2% in SDM and 107% in TDM. Moreover, the treatment also led to a significant enhancement in B accumulation in eucalyptus leaves, with increase values of 69.7% in RYL Oxisol and 84.5% in DRL Oxisol. These results clearly exceed the performances of treatments using BA alone, showing remarkable productivity with dry matter yields reaching 31 (g pot^{-1}) in RYL Oxisol and 36 (g pot^{-1}) in DRL Oxisol. This highlights the composites' efficacy in improving nutrition and growth in eucalyptus plants. It is important to note, however, that while the composites contribute significantly to growth, the total N content delivered via the composites is relatively low. Furthermore, the N available from these composites is either unavailable or only minimally available to eucalyptus.

The dynamics of B availability in soil, a critical factor for root absorption, varied significantly in the first 30 days, underlining the importance of composite choice for sustained B release, illustrating the importance of precipitation-dissolution and adsorption–desorption processes [79] and/or organic complex formation and

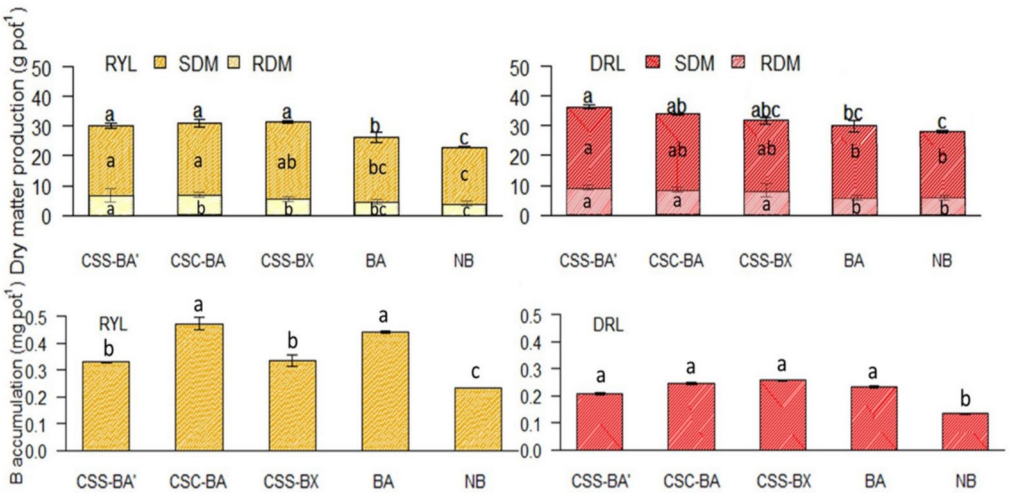

Fig. 6 Impact of fertilization with composites on eucalyptus growth characteristics and B nutrition in contrasting Oxisols: a study of aerial (SDM) and root dry matter production (RDM), B-accumulation in Eucalyptus and total production. In the graph, the solid bar represents total dry matter production (TDM). Dystrophic red-yellow latosol (RYL) and Dystrophic red latosol (DRL). Lowercase letters were used to compare the means of each parameter evaluated between treatments using the Tukey test ($p < 0.05$)

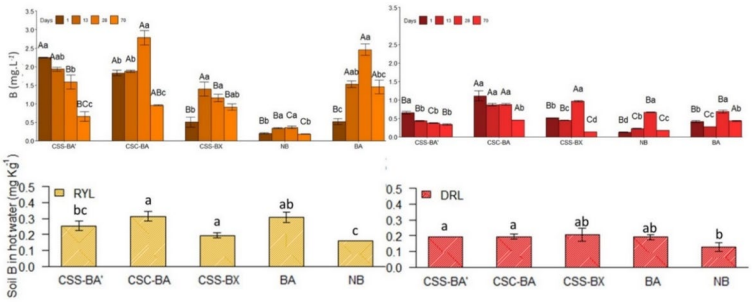

Fig. 7 Impact of fertilization with composites and boric acids on the availability of B (mg L^{-1}) and B in contrasting Oxisols cultivated with Eucalyptus (mg kg^{-1}). CSS-BA': sewage sludge + boric acid at 550 °C; CSC-BA: shrimp waste + boric acid at 300 °C; CSS-BX: sewage sludge + borax at 300 °C; BA: Boric Acid; NB: No B. Dystrophic red-yellow latosol (RYL) and Dystrophic red latosol (DRL). Lowercase letters were used to compare the means of each parameter evaluated between treatments using the Tukey test ($p < 0.05$)

soil organic matter [80]. RYL showed higher B availability compared to DRL soil, affecting the extraction sequence by the composites (Fig. 7).

Doping the FSC biochar matrix with B benefited the eucalyptus plants. B ensures greater preservation of N in the biochar and possibly increases chemical stability of C functional groups in the carbonized matrices, as shown in previous studies [14]. Moreover, groups ensuring higher CEC and adsorption capacity of composites are preserved when B is adsorbed through complexation due to the high ionization and selectivity of adsorbents [14]. Thus, synergy can accelerate eucalyptus development, ensuring a greater offer of B in controlled optimization of crop nutrition. Moreover, the composite can directly impact nutrient absorption and physiological processes, possibly improving drought tolerance through modulation of H^+ and ATP activity. This function of B contributes to B accumulation by the crop, with treatments surpassing NB [81]. The capacity of B-doped biochar composites to promote chemical stability and increase CEC reinforces the viability these materials possess in improving the nutrition and growth of Eucalyptus [14].

The availability of B in the soil was significantly impacted in the NB treatment, but the application of composites enhanced B availability. This contributed to the soil's ability to maintain optimal B levels for successive harvests [44], particularly those enriched with B sources [82]. Nevertheless, the significance of B extends beyond its role as a plant nutrient; it also contributes to the formation of organic composites that exhibit prolonged stability in the soil.

In this study, applications of CSC-BA were observed to enhance TDM and RDM significantly (Fig. 6). Additionally, this treatment markedly improves the solubility and accumulation of B in plants (Fig. 7). These findings indicate a high adaptability of CSC-BA to various soil conditions, which is crucial for effective nutrient management. The noted improvements in plant growth and photosynthetic efficiency can largely be attributed to the increased mobility of B—a critical element in soils susceptible to nutrient leaching. Customizing these treatments enhances soil quality significantly, promotes C sequestration and reduces dependence on chemical fertilizers, thereby bolstering sustainable agricultural practices [83]. Adapting agricultural management strategies to integrate precise B treatments according to local soil characteristics is vital for promoting the sustainable growth of eucalyptus plantations. Future research should focus on corroborating these findings in diverse environmental conditions and extending observational periods to fully ascertain the long-term impacts and efficacy of such tailored treatments.

Conclusions

This study demonstrates that the efficiency of boron (B) solubilization and release is significantly influenced by feedstock type, pyrolysis conditions and the form of B utilized. Nitrogen-rich feedstocks, particularly at 300 °C, were found to enhance B stabilization and performance in composites, effectively reducing volatilization losses. FTIR spectroscopy confirmed successful B integration into the carbon matrix via B–O and B–C bonds. Composites derived from boric acid (BA) exhibited superior molecular configurations, enhancing B release dynamics compared to those derived from borax (BX). Predictive PLS-FTIR models provided rapid and non-destructive characterizations of B within composites.

Incorporating B via BA before pyrolysis significantly improved composite properties, moderating B leachate in water and enhancing solution release dynamics. This showcases the potential these composites have of enhancing eucalyptus nutrition and growth in Oxisols.

CSC-BA composites, in particular, maintained B availability in Oxisols with low organic matter, supporting extended cultivation periods and successive plantings.

Future investigations should validate these findings through field applications under practical agricultural conditions. Research should also focus on formulating application methods for composites in different cropping systems. Additionally, long-term studies are needed to assess the environmental impacts and economic viability of B-biochar composites in sustainable agriculture.

Supplementary Information

The online version contains supplementary material available at https://doi.org/10.1186/s40538-024-00645-2.

Supplementary Material 1.

Acknowledgements
This work was financially supported by the CAPES agencies (CAPES-PROEX/AUXPE 593/2018), CNPq and FAPEMIG, for the funding and research grants granted. The Universidade Federal de Lavras (UFLA) is a provider of opportunities. L.C.A. Melo and C.A. Silva are research fellows of the National Council for Scientific and Technological Development (CNPq—Processes No. 311634/2021-4, 311212/2023-9, and 307447/2019-7). Keiji Jindo thanks the Agrosystems Research Group of Wageningen University and Research for the financial support (3710473400). L. Chisté acknowledges Dr. Everton Morais for the data analyses and support, Dr. Lívia Botelho and Dr. Mariene Duarte for the help with laboratory analyses and also thanks José Roberto Fernandes for the help with conducting experiments.

Author contributions
L. Chisté conducted the research, wrote the main manuscript text, prepared figures and tables, and edited and revised the manuscript. L.C.A. Melo supervised the work, reviewed the manuscript, and provided input. K. Jindo also reviewed the manuscript and provided input. C.A. Silva supervised the work, managed the project administration and funding acquisition, reviewed the manuscript, and provided input. All authors have reviewed the manuscript.

Funding
This research was funded by the Coordination for the Improvement of Higher Education Personnel (CAPES), CAPES-PROEX/AUXPE 593/2018 Scholarship, the National Council for Scientific and Technological Development (CNPq) and the Minas Gerais State Research Support Foundation (FAPEMIG).

Data availability
No datasets were generated or analyzed during the current study.

Declarations

Ethics approval and consent to participate
Not applicable.

Consent for publication
Not applicable.

Competing interests
The authors declare that they have no known competing financial interests or personal relationships that could have influenced the work reported in this paper.

Author details
[1]Department of Soil Science, School of Agricultural Sciences, Federal University of Lavras, Lavras, Minas Gerais 37200-900, Brazil. [2]Agrosystems Research, Wageningen University & Research, P.O. Box 16, 6700 AA Wageningen, The Netherlands.

Received: 23 April 2024 Accepted: 6 August 2024
Published online: 10 October 2024

References

1. R Mello Prado de 2021 Boron BT—mineral nutrition of tropical plants Springer International Publishing Cham 175 190 https://doi.org/10.1007/978-3-030-71262-4_10
2. SK Jha VK Mishra T Damodaran AK Singh YP Singh DK Sharma 2022 Does conservation tillage on partially reclaimed sodic soil restore land degradation by influencing boron dynamics, bioavailability for plant's uptake and nutritional security? Land Degrad Dev 33 1260 1268 https://doi.org/10.1002/ldr.4206
3. ASS Damasceno da CL Boechat HA Souza de GF Capristo-Silva WS Mendes de PE Teodoro 2023 Nutritional monitoring of boron in Eucalyptus spp in the Brazilian cerrado by multispectral bands of the MSI sensor (Sentinel-2) Remote Sens Appl Soc Environ. 29 100913
4. Z Chen Q Xu L Yan Y Wang A Sun Q Liu 2024 Fractionation of stable boron isotopes in alfisols: application of a novel tool for tracing boron behavior in two soil profiles Geoderma 441 116766
5. J Zhang A Koubaa D Xing W Liu Q Wang X Wang 2020 Improving lignocellulose thermal stability by chemical modification with boric acid for incorporating into polyamide Mater Des 191 108589
6. B Liu W Guo H Wang Q Si Q Zhao H Luo 2020 B-doped graphitic porous biochar with enhanced surface affinity and electron transfer for efficient peroxydisulfate activation Chem Eng J 396 125119
7. Q Huang S Song Z Chen B Hu J Chen X Wang 2019 Biochar-based materials and their applications in removal of organic contaminants from wastewater: state-of-the-art review Biochar. 1 45 73 https://doi.org/10.1007/s42773-019-00006-5
8. Y Ding Y Liu S Liu X Huang Z Li X Tan 2017 Potential benefits of biochar in agricultural soils: a review Pedosphere 27 645 661
9. W Hao P Luo Z Wu Y Mi Z Gao 2021 The effect of biomass pyrolysis temperature on the performance of biochar-fed molten hydroxide direct carbon fuel cells Biomass Bioenergy 150 106122 https://doi.org/10.1016/j.biombioe.2021.106122
10. M Luo C Zhu Q Chen F Song W Hao Z Shen 2023 In-situ growth of ZIF-8 nanocrystals on biochar for boron adsorption Colloids Surf A Physicochem Eng Asp 657 130504
11. WM Faria CC Figueiredo de TR Coser AT Vale BG Schneider 2018 Is sewage sludge biochar capable of replacing inorganic fertilizers for corn production? Evidence from a two-year field experiment Arch Agron Soil Sci. 64 505 519 https://doi.org/10.1080/03650340.2017.1360488
12. A Amaral Leite do AA Souza Cardoso de R Almeida Leite de AMV Barrera DDL Queiroz TC Viana 2024 Phosphate-solubilizing bacteria increase maize phosphorus uptake from magnesium-enriched poultry manure biochar Biol Fertil Soils 60 421 436 https://doi.org/10.1007/s00374-024-01808-x
13. I Paiva Oliveira de EG Morais de K Jindo CA Silva 2024 Biochar N content, pools and aromaticity as affected by feedstock and pyrolysis temperature Waste Biomass Valor. https://doi.org/10.1007/s12649-023-02415-x
14. G Pan J Wei M Xu J Li L Wang Y Li 2023 Insight into boron-doped biochar as efficient metal-free catalyst for peroxymonosulfate activation: Important role of -O-B-O- moieties J Hazard Mater 445 130479 https://doi.org/10.1016/j.jhazmat.2022.130479
15. X Zhang B Zhao H Liu Y Zhao L Li 2022 Effects of pyrolysis temperature on biochar's characteristics and speciation and environmental risks of heavy metals in sewage sludge biochars Environ Technol Innov 26 102288 https://doi.org/10.1016/j.eti.2022.102288
16. CT Johnston 2017 Biochar analysis by Fourier-transform infra-red spectroscopy B Singh M Camps-Arbestain J Lehmann Eds Biochar A guid to anal methods CRC Press/Taylor and Francis Group, LLC Boca Raton 199 213
17. ASTM International 1984 Standard test method for chemical analysis of wood charcoal—designation: D 1762–84 (reapproved 2001) Annu B ASTM Stand. 84 292 3
18. Singh B, Camps-Arbestain M, Lehmann J. Biochar: a guide to analytical methods. 2017.

19. O Mašek W Buss S Sohi 2018 Standard biochar materials Environ Sci Technol 52 9543 9544
20. NIST-SRM-1573a. Standard reference material 1573-Tomato leaves. 2018. p. 1–6.
21. Brasil. Manual De Métodos Analíticos oficiais para fertilizantes e corretivos. 2014.
22. D Liberda E Pięta K Pogoda N Piergies M Roman P Koziol 2021 The impact of preprocessing methods for a successful prostate cell lines discrimination using partial least squares regression and discriminant analysis based on Fourier transform infrared imaging Cells 10 953
23. Khan A, Harfield D, Hillen B, Stenzel F, Homung A. Long-termaging of biochar. 2017. http://dc.engconfintl.org/biochar/49/.
24. Teixeira PC, Donagemma GK, Fontana A, Teixeira WG. Manual de Métodos de Análise de Solo 3ª edição revista e ampliada. Man métodos análise solo - Capítulo 8 - Densidade partículas. 2017;574.
25. DL do Carmo CA Silva JM Lima de GL Pinheiro 2016 Electrical conductivity and chemical composition of soil solution: comparison of solution samplers in tropical soils Rev Bras Ciência do Solo https://doi.org/10.1590/18069657rbcs20140795
26. Silva FC da. Manual de análises químicas de solos, plantas e fertilizantes. Empres. Bras. Pesqui. Agropecuária Embrapa Solos Embrapa Informática Agropecuária Ministério da Agric. Pecuária e Abast. 2009.
27. R-Core-Team 2020 R: A language and environment for statistical computing R Foundation for Statistical Computing Vienna
28. R Kiralj MMC Ferreira 2009 Basic validation procedures for regression models in QSAR and QSPR studies: theory and application J Braz Chem Soc 20 770 787
29. PP Roy S Paul I Mitra K Roy 2009 On two novel parameters for validation of predictive QSAR models Molecules 14 1660 1701
30. H Akaike 1979 A Bayesian extension of the minimum AIC procedure of autoregressive model fitting Biometrika 66 237 242 https://doi.org/10.1093/biomet/66.2.237
31. L Leng S Xu R Liu T Yu X Zhuo S Leng 2020 Nitrogen containing functional groups of biochar: an overview Bioresour Technol 298 122286
32. MI Piash K Iwabuchi T Itoh 2022 Synthesizing biochar-based fertilizer with sustained phosphorus and potassium release: co-pyrolysis of nutrient-rich chicken manure and Ca-bentonite Sci Total Environ 822 153509
33. AA Almutairi M Ahmad MI Rafique MI Al-Wabel 2023 Variations in composition and stability of biochars derived from different feedstock types at varying pyrolysis temperature J Saudi Soc Agric Sci 22 25 34
34. RR Domingues PF Trugilho CA Silva ICNA Melo de LCA Melo ZM Magriotis 2017 Properties of biochar derived from wood and high-nutrient biomasses with the aim of agronomic and environmental benefits PLoS ONE 12 e0176884 https://doi.org/10.1371/journal.pone.0176884
35. JSS Carneiro da ICA Ribeiro BO Nardis CF Barbosa JF LustosaFilho LCA Melo 2021 Long-term effect of biochar-based fertilizers application in tropical soil: agronomic efficiency and phosphorus availability Sci Total Environ 760 143955 https://doi.org/10.1016/j.scitotenv.2020.143955
36. OA Salawu Z Han AS Adeleye 2022 Shrimp waste-derived porous carbon adsorbent: performance, mechanism, and application of machine learning J Hazard Mater 437 129266
37. JA Ippolito L Cui C Kammann N Wrage-Mönnig JM Estavillo T Fuertes-Mendizabal 2020 Feedstock choice, pyrolysis temperature and type influence biochar characteristics: a comprehensive meta-data analysis review Biochar 1 421 438 https://doi.org/10.1007/s42773-020-00067-x
38. MI Rafique ARA Usman M Ahmad A Sallam MI Al-Wabel 2020 In situ immobilization of Cr and its availability to maize plants in tannery waste–contaminated soil: effects of biochar feedstock and pyrolysis temperature J Soils Sediments 20 330 339 https://doi.org/10.1007/s11368-019-02399-z
39. C Chen LL Zhou YN Huang WK Wang J Xu 2022 Boron regulates catalytic sites of biochar to enhance the formation of surface-confined complex for improved peroxydisulfate activation Chemosphere 301 134690
40. S Kim U Kim J Ryu D Kim M Kim YC Joo 2023 Boron-doped amorphous carbon deposited by DC sputtering for a hardmask: microstructure and dry etching properties Appl Surf Sci 637 157895
41. Z Yang Z Yao G Li G Fang H Nie Z Liu 2011 Sulfur-doped graphene as an efficient metal-free cathode catalyst for oxygen reduction ACS Nano. https://doi.org/10.1021/nn203393d
42. H Zhang Q Cao K Zhang L Xie K Xu Y Qin 2023 Boron-doped biochar-nano loaded zero-valent iron to activate persulfate for the degradation of oxytetracycline J Environ Chem Eng 11 111502
43. X Bo L Guo 2013 Carbonos mesoporosos dopados com boro ordenados como eletrocatalisadores isentos de metal para a reação de redução de oxigênio em solução alcalina Phys Chem Chem Phys 15 2459 2465
44. MP Schmidt SD Siciliano D Peak 2021 The role of monodentate tetrahedral borate complexes in boric acid binding to a soil organic matter analogue Chemosphere 276 130150 https://doi.org/10.1016/j.chemosphere.2021.130150
45. J Huang Y Zhu H Bian L Song Y Liu Y Lv 2023 Insights into enhanced peroxydisulfate activation with B and Fe co-doped biochar from bark for the rapid degradation of guaiacol Molecules 28 7591
46. F Yang C Wang H Sun 2021 A comprehensive review of biochar-derived dissolved matters in biochar application: production, characteristics, and potential environmental effects and mechanisms J Environ Chem Eng 9 105258
47. S Saha MT Islam J Calhoun T Reza 2023 Effect of hydrothermal carbonization on fuel and combustion properties of shrimp shell waste Energies 16 5534
48. RH Rødde A Einbu KM Vårum 2008 A seasonal study of the chemical composition and chitin quality of shrimp shells obtained from northern shrimp (*Pandalus borealis*) Carbohydr Polym 71 388 393
49. Y Gao Q Wang G Ji A Li J Niu 2021 Doping strategy, properties and application of heteroatom-doped ordered mesoporous carbon RSC Adv 11 5361 5383 https://doi.org/10.1039/D0RA08993A
50. D Wu F Sun Z Qu H Wang Z Lou B Wu 2022 Multi-scale structure optimization of boron-doped hard carbon nanospheres boosting the plateau capacity for high performance sodium ion batteries J Mater Chem A. 10 17225 17236 https://doi.org/10.1039/D2TA04194D
51. Z Wang X Xu S Ma H Wang H Zhao Y Wang 2021 The superior adsorption capacity of boron-nitrogen co-doping walnut shell biochar powder for Au(III), Pt(IV), and Pd(II) J Environ Chem Eng 9 106288
52. A Haque RA Al-Balushi PR Raithby MS Khan 2020 Recent advances in π-conjugated N^C-chelate organoboron materials Molecules 25 2645
53. L Sui C Tang Q Du Y Zhao K Cheng F Yang 2021 Preparation and characterization of boron-doped corn straw biochar: Fe (II) removal equilibrium and kinetics J Environ Sci 106 116 123
54. I Waclawska 1995 Thermal decomposition of borax J Therm Anal 43 261 269 https://doi.org/10.1007/BF02635993
55. R Labanya PC Srivastava SP Pachauri AK Shukla M Shrivastava P Mukherjee 2022 Sorption–desorption of some transition metals, boron and sulphur in a multi-ionic system onto phyto-biochars prepared at two pyrolysis temperatures Environ Sci Process Impacts 24 2378 2397 https://doi.org/10.1039/D2EM00212D
56. F Shireen MA Nawaz C Chen Q Zhang Z Zheng H Sohail 2018 Boron: functions and approaches to enhance its availability in plants for sustainable agriculture Int J Mol Sci 19 1856
57. J Omiri Y Snoussi AK Bhakta S Truong S Ammar AM Khalil 2022 Citric-acid-assisted preparation of biochar loaded with copper/nickel bimetallic nanoparticles for dye degradation Colloids Interfaces. 6 18
58. EG Morais K Jindo CA Silva 2023 Biochar-based phosphate fertilizers: synthesis, properties, kinetics of p release and recommendation for crops grown in oxisols Agronomy 13 326
59. Y Du M Dai I Naz X Hao X Wei R Rong 2021 Carbothermal reduction synthesis of zero-valent iron and its application as a persulfate activator for ciprofloxacin degradation Sep Purif Technol 275 119201 https://doi.org/10.1016/j.seppur.2021.119201
60. A Ateş B Aydemir KE Öksüz 2023 Investigation of physicochemical and biological properties of boron-doped biochar Biomass Convers Bioref. https://doi.org/10.1007/s13399-023-04567-1
61. M Jia F Wang Y Bian X Jin Y Song FO Kengara 2013 Effects of pH and metal ions on oxytetracycline sorption to maize-straw-derived biochar Bioresour Technol 136 87 93
62. Y Zhou W Yan X Yu T Chen S Wang W Zhao 2020 Boron and nitrogen co-doped porous carbon for supercapacitors: a comparison between a microwave-assisted and a conventional hydrothermal process J Energy Storage. 32 101706 https://doi.org/10.1016/j.est.2020.101706
63. F Sun Z Qu J Gao WuH Bin F Liu R Han 2018 In situ doping boron atoms into porous carbon nanoparticles with increased oxygen graft enhances both affinity and durability toward electrolyte for greatly improved supercapacitive performance Adv Funct Mater. 28 1804190

64. J Quílez-Bermejo E Morallón D Cazorla-Amorós 2020 Metal-free heteroatom-doped carbon-based catalysts for ORR: a critical assessment about the role of heteroatoms Carbon NY 165 434 454
65. N Friedrich P Brandimarte J Li S Saito S Yamaguchi I Pozo 2020 Magnetism of topological boundary states induced by boron substitution in graphene nanoribbons Phys Rev Lett 125 146801
66. X Zhang DD Gang J Zhang X Lei Q Lian WE Holmes 2022 Insight into the activation mechanisms of biochar by boric acid and its application for the removal of sulfamethoxazole J Hazard Mater 424 127333
67. K Nakamoto 2009 Infrared and Raman spectra of inorganic and coordination compounds, part B: applications in coordination, organometallic, and bioinorganic chemistry Wiley Hoboken
68. H Wang Y Dong Y Yang GS Toor X Zhang 2013 Changes in heavy metal contents in animal feeds and manures in an intensive animal production region of China J Environ Sci 25 2435 2442
69. C Wang C Huang J Qian J Xiao H Li Y Wen 2014 Rapid and accurate evaluation of the quality of commercial organic fertilizers using near infrared spectroscopy PLoS ONE 9 e88279 https://doi.org/10.1371/journal.pone.0088279
70. J Ruangratanakorn T Suwonsichon S Kasemsumran W Thanapase 2020 Installation design of on-line near infrared spectroscopy for the production of compound fertilizer Vib Spectrosc 106 103008
71. X Yue L Fei-Yue F Xing-Jun H Shui-Jin X Xin W Jian-Fei 2018 Cite this article as: Chinese Chin J Anal Chem 46 609 615
72. H Yang K Sheng 2012 Characterization of biochar properties affected by different pyrolysis temperatures using visible-near-infrared spectroscopy Int Sch Res Netw ISRN Spectrosc. 2012 1 7
73. F Sun HB Wu X Liu F Liu R Han Z Qu 2018 A high-rate and ultrastable anode enabled by boron-doped nanoporous carbon spheres for high-power and long life lithium ion capacitors Mater Today Energy. https://doi.org/10.1016/j.mtener.2018.07.009
74. L Xu Y Qi S He C Wang X Jin Q Wang 2025 Facile synthesis of boron-doped porous biochar as a metal-free adsorbent for efficient removal of aqueous tetracycline antibiotics J Environ Sci 152 235 247
75. JF Lustosa Filho ES Penido PP Castro CA Silva LCA Melo 2017 Co-pyrolysis of poultry litter and phosphate and magnesium generates alternative slow-release fertilizer suitable for tropical soils ACS Sustain Chem Eng. 5 9043 9052 https://doi.org/10.1021/acssuschemeng.7b01935
76. H Werheit T Au R Schmechel SO Shalamberidze GI Kalandadze AM Eristavi 2000 IR-active phonons and structure elements of isotope-enriched boron carbide J Solid State Chem 154 79 86
77. V Thirumal A Pandurangan R Jayavel R Ilangovan 2016 Synthesis and characterization of boron doped graphene nanosheets for supercapacitor applications Synth Met https://doi.org/10.1016/j.synthmet.2016.07.011
78. BER Hodecker NF Barros De IR Silva Da V Diola JES Sarkis ME Loureiro 2014 Boron delays dehydration and stimulates root growth in Eucalyptus urophylla (Blake, S.T.) under osmotic stress Plant Soil 384 185 199 https://doi.org/10.1007/s11104-014-2196-4
79. I Bhupenchandra A Basumatary S Dutta LK Singh N Datta 2020 Impact of boron fertilization on boron fractions at different crop growth stages in cauliflower_cowpea_okra sequence in an inceptisols of North East India J Plant Nutr 43 1175 1188
80. K Hansson JP Laclau L Saint-André L Mareschal G Heijden van der C Nys 2020 Fertilidade química dos ecossistemas florestais. Parte 1: Análises químicas comuns do solo foram preditores fracos da produtividade do povoamento em uma ampla gama de solos florestais ácidos Ecol e manejo Florest. 461 117843
81. GA Ferreira FWR Hippler LAS Prado do JAH Rima RM Boaretto JA Quaggio 2021 Boron modulates the plasma membrane H+-ATPase activity affecting nutrient uptake of Citrus trees Ann Appl Biol 178 293 303
82. I Bhupenchandra A Basumatary S Dutta A Das AK Choudhary R Lal 2024 Repercussions of fertilization with boron and enriched organic manure on soil chemical characteristics, boron and phosphorus fractions, and French bean productivity in an acidic Inceptisol of eastern Himalaya Sci Hortic (Amsterdam). 324 304 4238 https://doi.org/10.1016/j.scienta.2023.112589
83. S Khan S Irshad K Mehmood Z Hasnain M Nawaz A Rais 2024 Biochar production and characteristics, its impacts on soil health, crop production, and yield enhancement: a review Plants 13 166

Publisher's Note